Supporting Information

High-performance Circularly Polarized Photodetectors Based on Chiral Transfer of Achiral Poly(9,9-dioctylfluorene)

Xiaocheng Wu[†‡], Junjie Liu[†‡], Yunhao Xu[†‡], Longzhen Qiu*[†‡], Xiaohong Wang*[†‡]

[†]National Engineering Lab of Special Display Technology, State Key Lab of Advanced Display Technology, Academy of Opto-Electronic Technology, Hefei University of Technology, Hefei 230009, P. R. China

[‡]Intelligent Interconnected Systems Laboratory of Anhui, Anhui Province Key Laboratory of Measuring Theory and Precision Instrument, School of Instrument Science and Optoelectronic Engineering, Hefei University of Technology, Hefei 230009, P. R. China

*Corresponding authors.

E-mail: xhwang11@hfut.edu.cn (X. Wang); lzhqiu@hfut.edu.cn (L. Qiu)

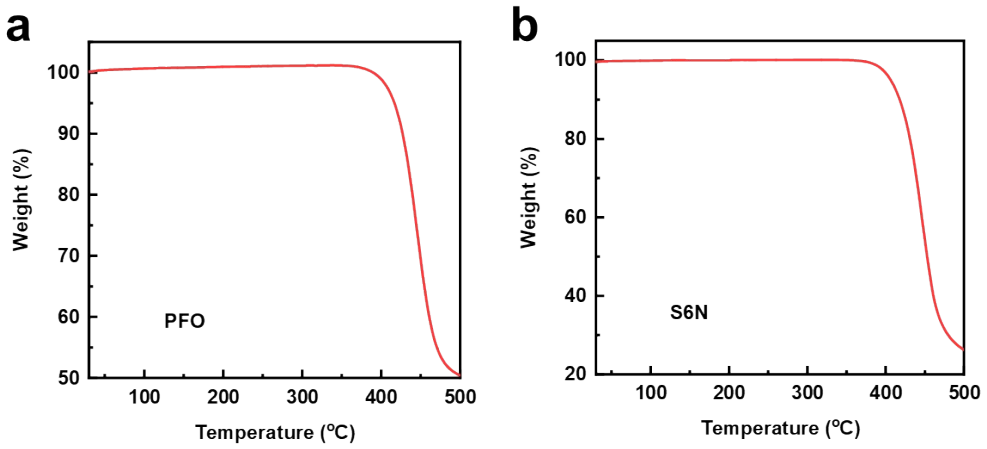

Figure S1. Thermogravimetric analysis curves of a) S6N, b) PFO.

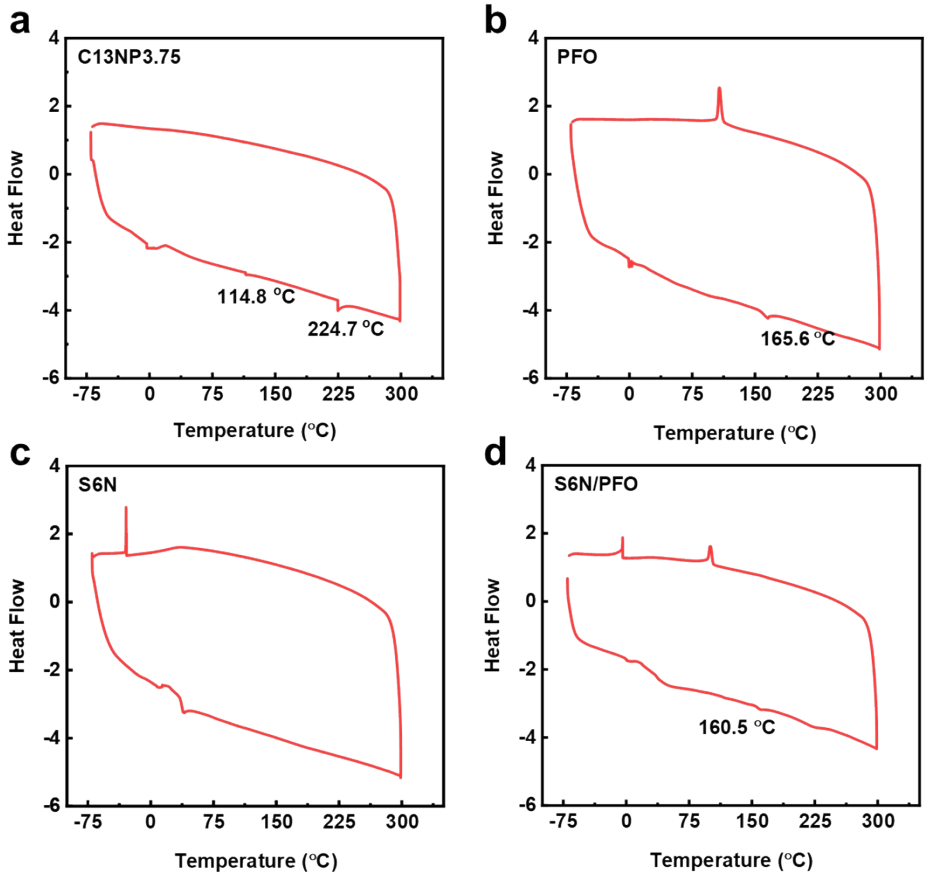

Figure S2. Raw data plot of DSC curves for a) C13P3.75, b) PFO, c) S6N, and d) S6N/PFO blended membranes.

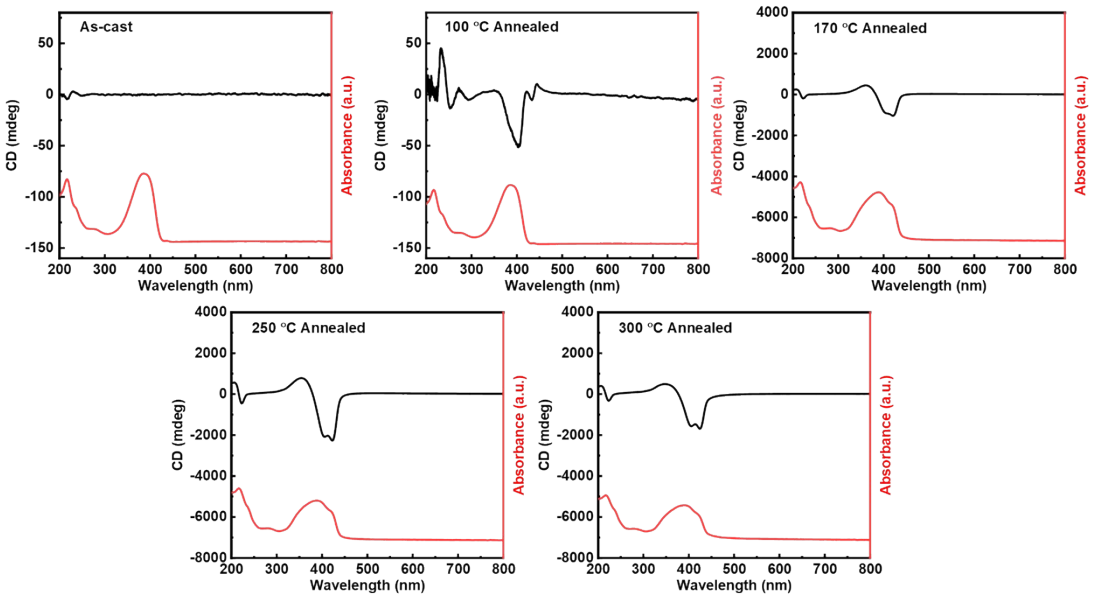

Figure S3. CD spectra and UV-Vis-NIR spectra of S6N/PFO blend films at different annealing temperatures. (PFO concentration 10 mg/mL and S6N content 10 wt%).

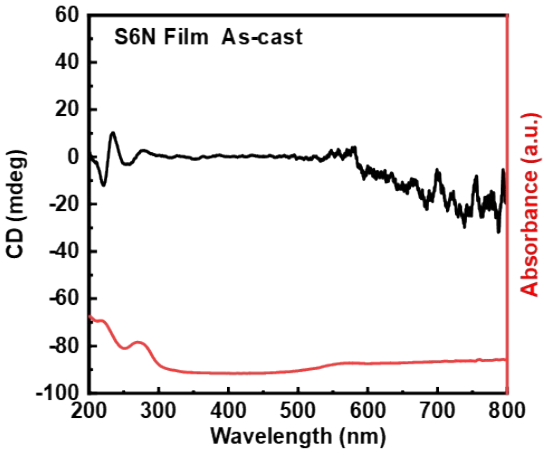

Figure S4. CD spectra and UV-Vis-NIR absorption spectra of S6N films under unannealed conditions. The CD signals and absorption peaks of S6N films are in the range of 200 nm-300 nm wavelength.

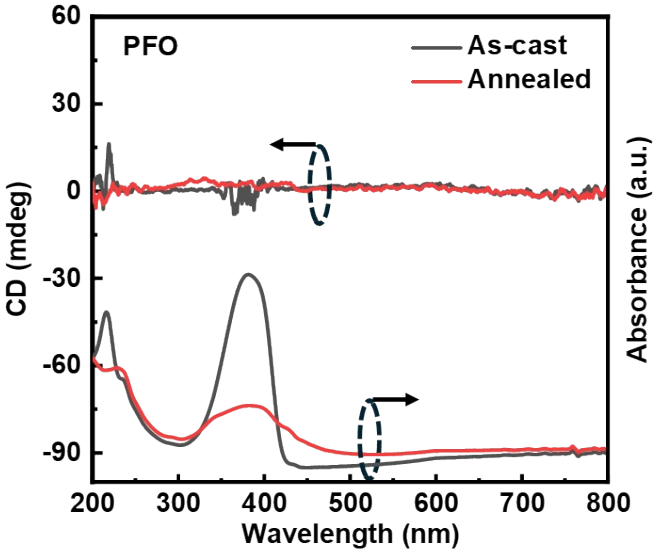

Figure S5. CD spectra and UV-Vis-NIR absorption spectra of PFO films at room temperature and annealed conditions.

The PFO films without the addition of S6N chiral small molecules did not exhibit CD signals at room temperature and after annealing, and the characteristic absorption peaks were all around 400 nm. In contrast, the blended films with the addition of S6N and annealing showed new CD signals in the range of 400-450 nm. These results indicate the successful realization of the blending-induced chiral transfer strategy. The CD signal around 400 nm is caused by the small molecule with axial chirality, S6N, affecting the molecular arrangement during the phase transition of PFO at high temperature.

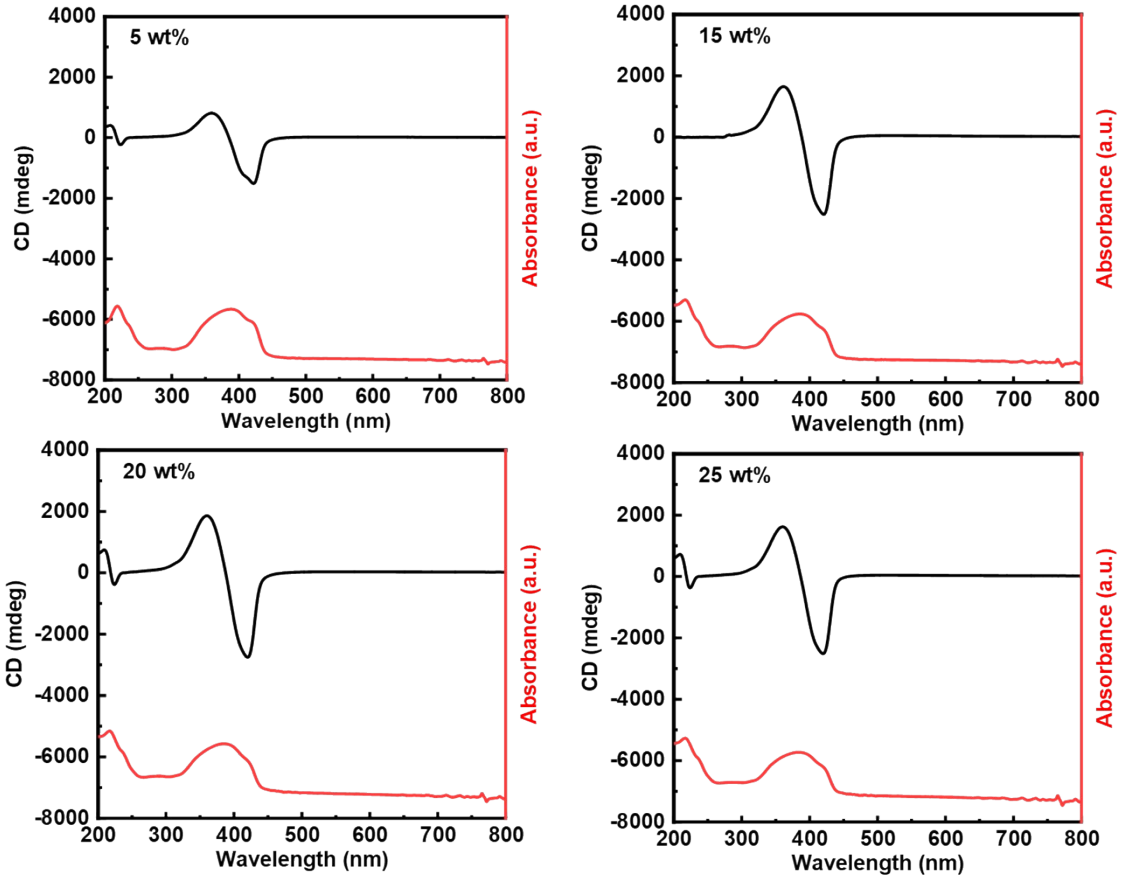

Figure S6. CD and UV-vis-NIR absorption spectra of blended films with different S6N contents after annealing at 250 °C.

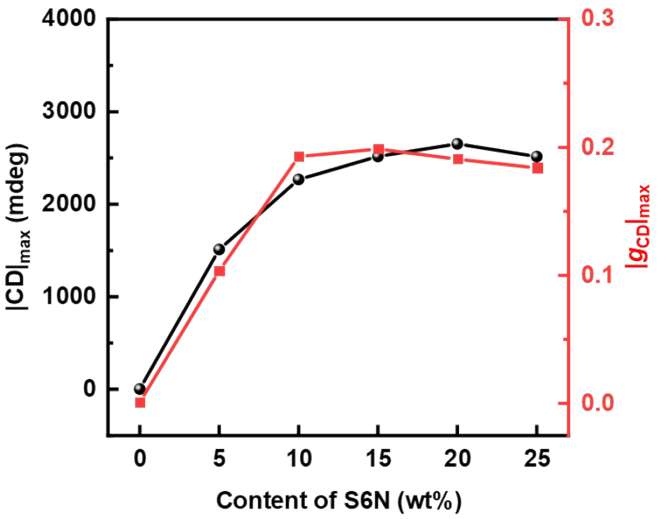

Figure S7. Statistics of maximum CD and g_{CD} values in the wavelength range of 400-425 nm after annealing at 250 °C for blended films with different S6N contents.

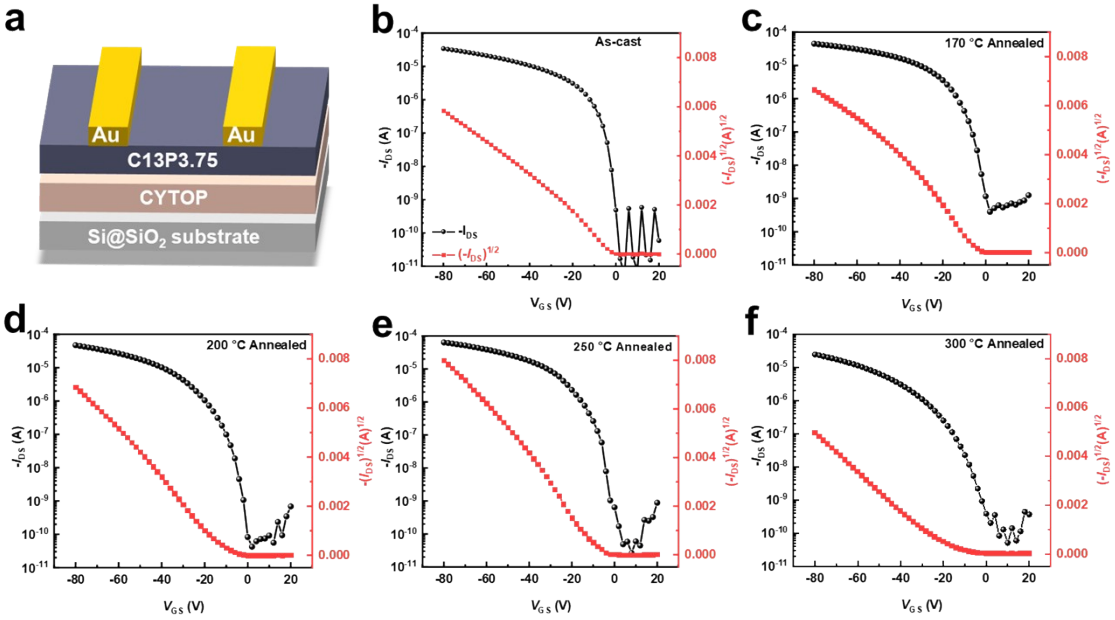

Figure S8. a) Schematic diagram of the structure of a single-layer C13P3.75 semiconductor film organic field effect transistor device. b)-f) Characterization of electrical properties of devices under different annealing temperature conditions.

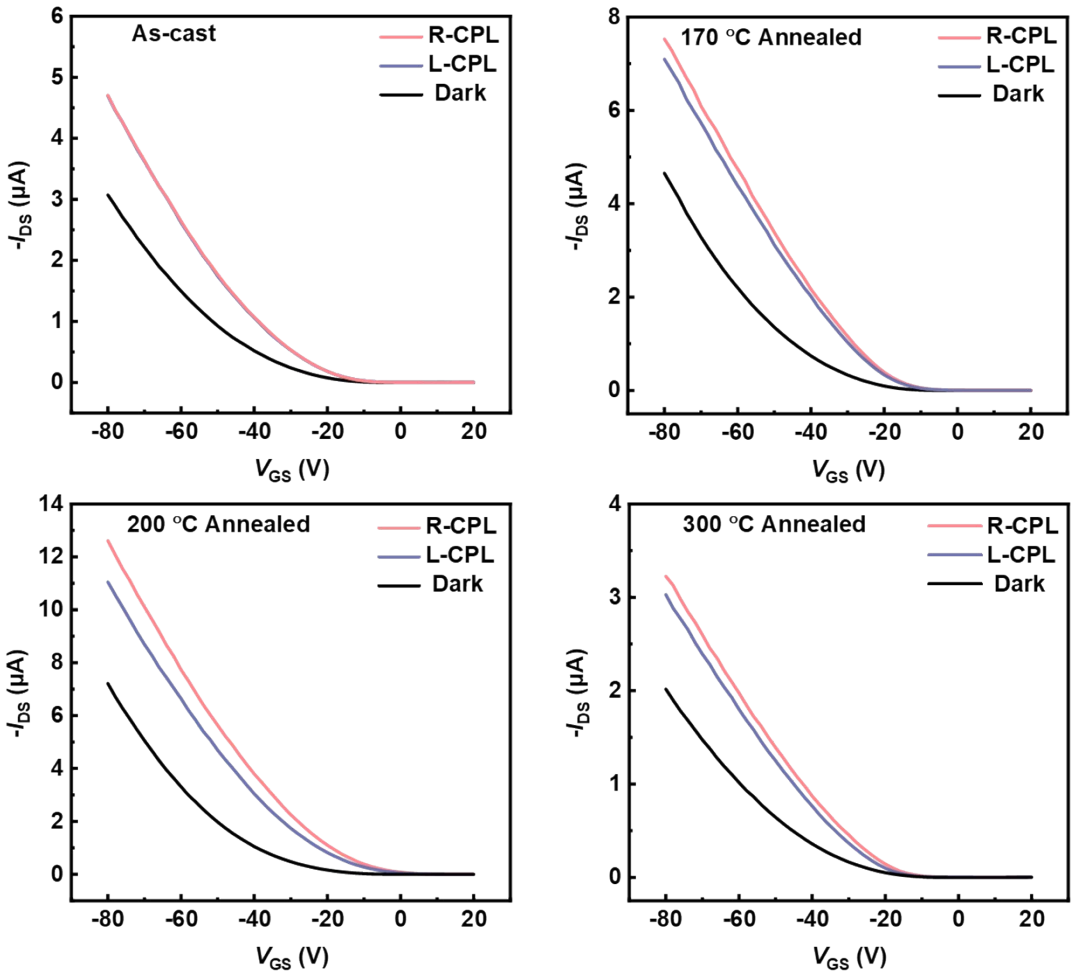

Figure S9. Characterization of the electrical properties of bilayer devices under different annealing conditions under dark and circularly polarized light irradiation. The blue and red curves represent left-rotated circularly polarized light and right-rotated circularly polarized light, respectively, and the difference between them is used to characterize the differentiation ability. The larger the difference, the better the ability of the device to discriminate circularly polarized light.

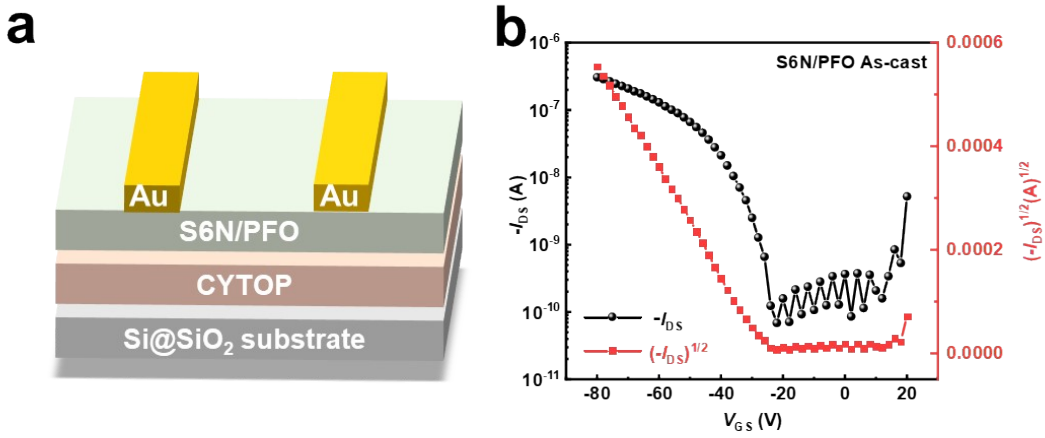

Figure S10. a) Charge transport layer device structure using only S6N/PFO. b) Transfer characteristic curve of the device with S6N/PFO as the charge transfer layer. (PFO concentration 10 mg/mL and S6N content 10 wt%).

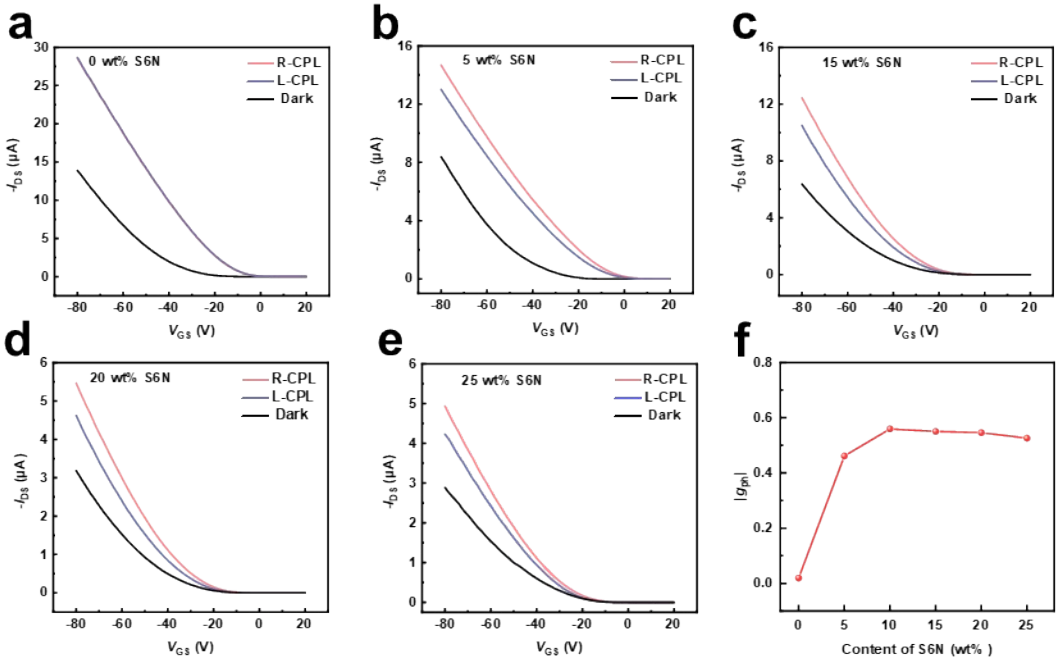

Figure S11. a)-e) Characterization of electrical properties and CPL differentiation ability of bilayer devices with different S6N contents under 250 °C annealing condition. f) Statistics of $|g_{ph}|$ values for devices with different S6N content at 250 °C annealing conditions (V_{DS} = -80 V, V_{GS} = -10 V).

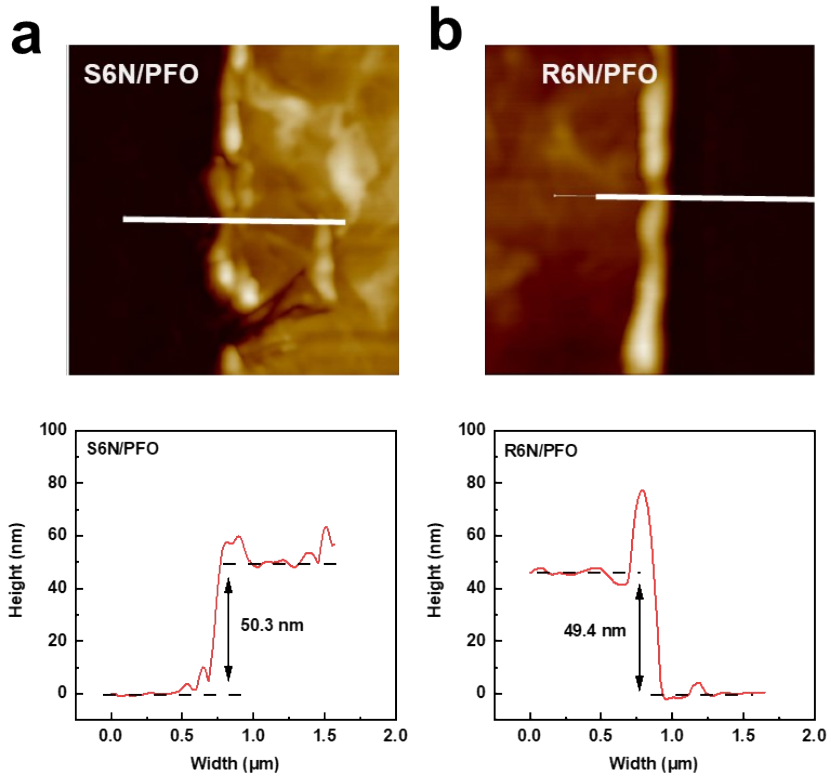

Figure S12. Measurement of blending film thickness by AFM: a) S6N/PFO film. b) R6N/PFO blend film.

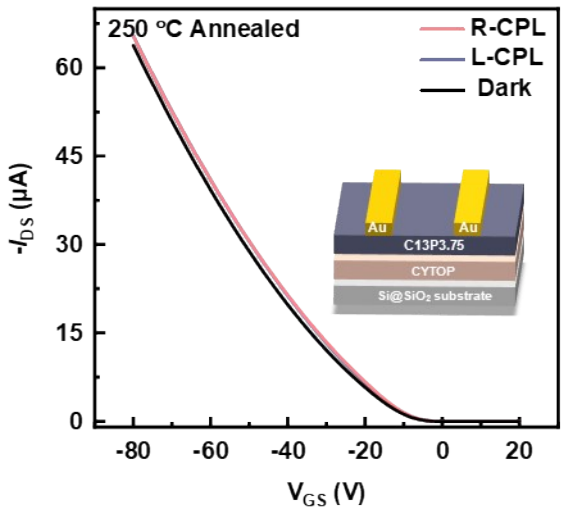

Figure S13. Characterization of the electrical properties of chiral-free sensing layer devices under irradiation with different rotationally circularly polarized light.

The overlapping red and blue curves indicate that the devices with only C13P3.75 as the charge transport layer and no chiral layer do not have circularly polarized light (CPL) differentiation ability. Comparison with the results for the bilayer device shows that the CPL differentiation ability of the bilateral device is conferred by the chiral co-hybrid layer.

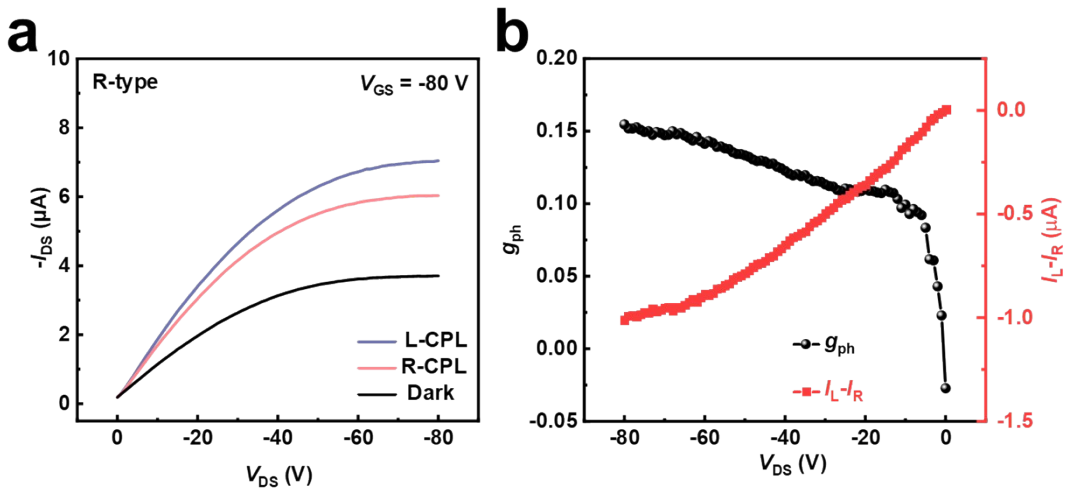

Figure S14. a) Output characteristic curve of R-type device; b) photocurrent asymmetry factor g_{ph} and photocurrent difference I_L-I_R of R-type device.

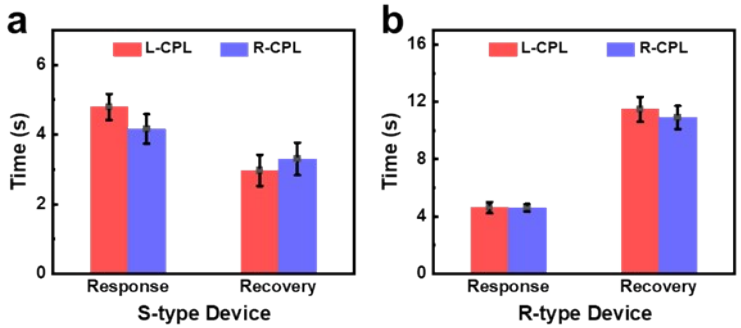

Figure S15. a) and b) Statistical plots of the time required for the current to rise and return to a steady state for S-type devices and R-type devices, respectively, under different rotational CPL optical pulses.

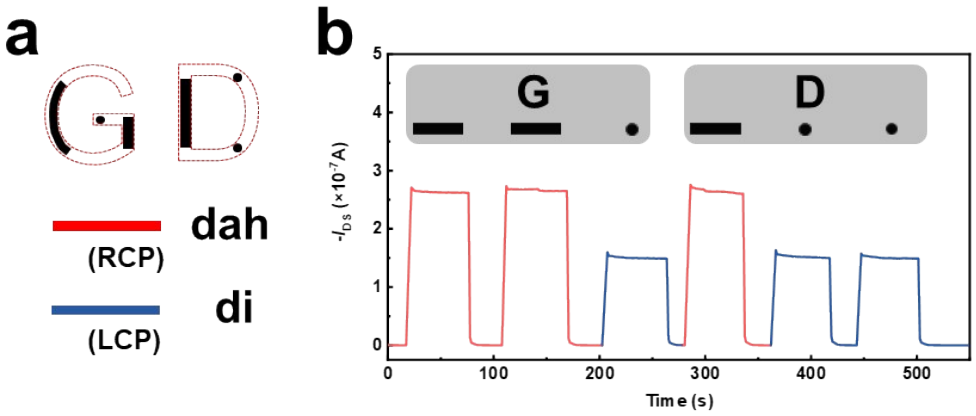

Figure S16. a) Schematic diagram of Morse code against alphabet. where the photocurrents under R-CPL and L-CPL conditions are regarded as long-dashed signal 'dah' and short-dotted signal 'di', respectively. b) Simulation of Morse code 'GD' utilizing a light program.

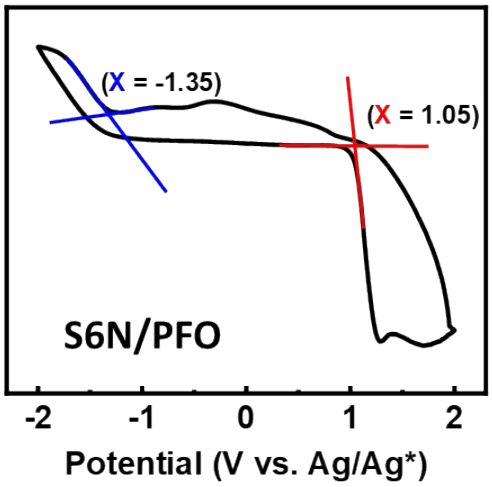

Figure S17. S6N/PFO redox potentials obtained by cyclic voltammetry

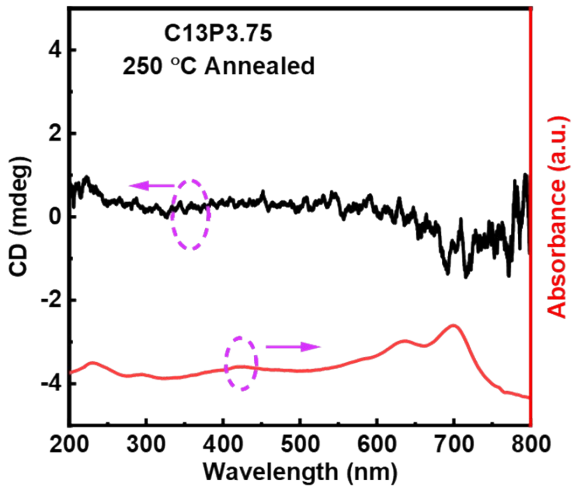

Figure S18. CD spectra and UV-Vis-NIR absorption spectra of the charge transport layer (C13P3.75) after annealing. The results show that C13P3.75 does not possess chiral optical activity and the absorption is mainly in the range of 600-750 nm.

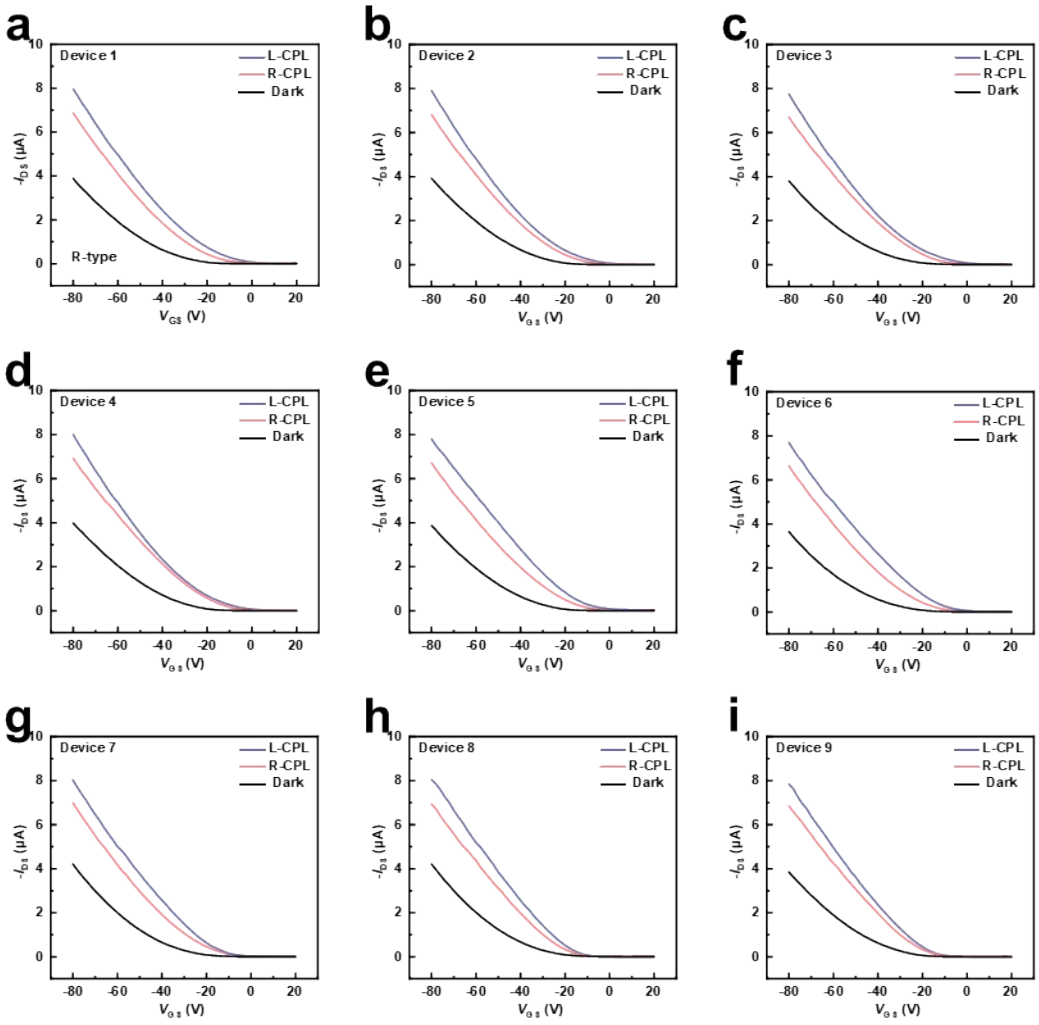

Figure S19. Transfer characteristic curves for each device in an R-type 3×3 device array under dark conditions, R-CPL irradiation, and L-CPL irradiation.